DISCLAIMER

This report was prepared as an account of work sponsored by an agency of the United States Government. Neither the United States Government nor any agency thereof, nor any of their employees, makes any warranty, express or implied, or assumes any legal liability or responsibility for the accuracy, completeness, or usefulness of any information, apparatus, product, or process disclosed, or represents that its use would not infringe privately owned rights. Reference herein to any specific commercial product, process, or service by trade name, trademark, manufacturer, or otherwise does not necessarily constitute or imply its endorsement, recommendation, or favoring by the United States Government or any agency thereof. The views and opinions of authors expressed herein do not necessarily state or reflect those of the United States Government or any agency thereof.

BNL--42064

DE89 004519

X-RAY REFLECTIVITY AND SURFACE ROUGHNESS

B.M. Ocko

Physics Department
Brookhaven National Laboratory
Upton, New York 11973

ABSTRACT. Since the advent of high brightness synchrotron radiation sources there has been a phenomenal growth in the use of x-rays as a probe of surface structure. The technique of x-ray reflectivity is particularly relevant to electrochemists since it is capable of probing the structure normal to an electrode surface in situ. In this paper the theoretical framework for x-ray reflectivity is reviewed and the results from previous non-electrochemistry measurements are summarized. These measurements are from the liquid/air interface (CCl_4), the metal crystal vacuum interface (Au(100)), and from the liquid/solid interface(liquid crystal/silicon).

1. INTRODUCTION

The surface structure of electrodes in electrolyte solutions is a fundamental problem in electrochemistry, catalysis and surface science. The arrangement of the atoms at the surface has a pronounced impact on the electronic structure and reactivity of the surface. Direct structural studies of electrode interfaces in-situ are not possible with conventional structural surface science techniques such as Low Energy Electron Diffraction (LEED). Recently several groups have realized the importance of x-rays as a direct structural probe in-situ and these efforts have utilized EXAFS[1, 2], Standing wave[3] and Glancing Incident Angle Diffraction[4] techniques at a number of synchrotron sources. X-ray reflectivity techniques probe the structure along the surface normal direction, including the effects of roughness. Since reflectivity techniques can also be applied in situ, they should play an important role in understanding electrochemical systems. These techniques will be applicable to the problems of surface reconstruction, underpotential deposition, and surface oxidation.

It is important to define the coordinate system before proceeding. We will choose the surface normal direction to be $\hat{z}$ and the two directions in the plane of the surface as $\hat{x}$ and $\hat{y}$. For specular reflectivity the scattering is aligned along the $\hat{z}$ direction. The momentum transfer $Q_z=(4\pi/\lambda)sin\,\theta$ where λ is the x-ray wavelength and θ is the incident angle with respect to the surface plane. Since specular scattering is confined to the $\hat{z}$ direction the

MASTER

DISTRIBUTION OF THIS DOCUMENT IS UNLIMITED

reflectivity is often referred to as a rod of scattering[5]. By measuring the specular reflectivity starting at very small θ and possibly extending out to Bragg peaks information on the structure along the surface normal direction is obtained. Fitting the data to simple surface models allows us to deduce the surface roughness, mass, and expansion(contraction) of the surface. For small incident angles the data can be modeled as a perturbation from a perfect interface and the corresponding deviation from the Fresnel Law of Optics.

Specular reflectivity techniques have been applied to a large variety of problems at solid and liquid interfaces. X-ray studies have been performed at the liquids surfaces of mercury[6, 7, 8], water[9], carbon tetrachloride and methanol[10], liquid crystals[11, 12, 13], microemulsions[14], on Langmuir films on water[15, 16, 17] and on thin water layers on solids. Experiments on solid surfaces include Au(100)[18], Cu(110)[19], silicon oxide interfaces[20] and on silanes coated silicon[21, 22] These same classes of experiments could also be explored at the air/electrolyte surface and on the metal/electrolyte surface.

This paper is divided into four sections. In this section the scattering geometry is outlined. In the next section we will consider a continuum model of the electron density. This approach is most applicable at small angles and provides a simple description of the reflectivity in terms of a deviation from the Fresnel Law. These deviations can be simply related to surface roughness effects and for simple liquids this roughness can be calculated from the surface tension of the liquid. In the third section, we will consider the scattering from discrete atoms. This is particularly useful in describing the structure of single crystal surfaces. In the final section, preliminary measurements at the liquid crystal/solid interface are presented.

Before turning to the continuum and discrete models, we will briefly discuss x-ray sources. X-rays are produced via a conventional fixed target tube source, via a rotating anode generator or by a synchrotron. The first two methods produce x-rays which exit from the source in all directions. A small collimated beam is chosen from slits which are located a distance from the source which is usually less than 1 meter. These slits are followed by a monochromator crystal, typically germanium or silicon, which is tuned to accept the intrinsic radiation from the source. The source is typically either copper or molybdenum and the characteristic lines are at 1.54 Å and 0.71 Å respectively. At a synchrotron source the divergence of the x-ray beam is controlled by the energy of the ring and is just $1/\gamma$. At NSLS this corresponds to 2.5×10^{-4} radians. To provide a monochromatic beam, the x-rays are Bragg reflected from single crystals. The intensity from current synchrotron sources at about 1 Angstrom is about one thousand times more intense then from a rotating anode, which is typically ten times brighter then a conventional tube source. In order to measure the specular reflectivity it is convenient to use a two circle x-ray goniometer which allows the incident and outgoing angles to be controlled independently. For liquid interfaces, the sample can not be tilted and the incident angle is controlled by tilting the incident beam downward and adjusting the sample height.

2. CONTINUUM MODELS (Liquid Surfaces)

In the continuum model, the index of refraction for materials is given by the free electron model[23] where the dielectric constant is given by

$$\epsilon = 1 - \frac{\rho_e \lambda^2}{\pi} \left(\frac{e^2}{mc^2} \right) \tag{1}$$

where ρ_e is the electron density, e is the electron charge, and m is the mass of an electron. The effect of absorption has been ignored which would give rise to an imaginary index of refraction. We will now consider a vacuum/solid interface in which the dielectric constant of the vacuum is unity and the dielectric constant of the solid is given by Eq. 1. For angles below the critical angle θ_c the x-rays are totally externally reflected according to Snell's Law. Solutions to Maxwell's Equations gives the intensity of the reflected field divided by the incident field. This is often referred to as the Fresnel Law of Optics. In the small angle approximation it is given by

$$R = \frac{|E_R|^2}{|E_0|^2} = \left| \frac{\theta_c}{\theta^2 + \sqrt{\theta^2 - \theta_c^2}} \right|^4 \tag{2}$$

where the critical angle for total external reflection

$$\theta_c = \sqrt{\rho_e^2 \lambda^2 / \pi mc^2} \tag{3}$$

shown by the solid line in figure 1. At angles below θ_c there is total external reflection. The critical wavevector $Q_c = (4\pi/\lambda)\theta_c$ is independent of wavelength. Numerically, $Q_c = 3.75 \times 10^{-14} \rho_e^{1/2}$ Å^{-1}, where ρ_e is in electrons/cm^3. It is convenient to rewrite Eq. 2 as

$$R = \left[\frac{\theta_c}{2\theta} \right]^4 |T(\theta)|^4 \tag{4}$$

where the enhancement factor

$$T(\theta) = \frac{2\sin\theta}{\sin\theta + \sqrt{\cos^2\theta_c - \cos^2\theta}}. \tag{5}$$

expresses the amount by which the electric field is enhanced at the interface. For θ several times θ_c the enhancement factor is very close to unity and the reflectivity can be well approximated by

$$R = \left[\frac{\theta_c}{2\theta}\right]^4 \tag{6}$$

which is shown by the dashed line in figure 1. At five times the critical angle the reflected intensity is slightly less than 10^{-5}.

For interfaces which are not ideally sharp (i.e. a diffuse interface) the reflectivity falls off faster than the θ^{-4} dependence given by the Fresnel Law. This can be understood physically by considering the interface as discrete slabs of dielectric material which mimic the actual electron density profile. This is a generalized extension of the technique to measure film thickness with ellipsometry.

For smoothly varying interfaces, the actual reflectivity can be calculated as a perturbation from the ideal step interface. The theoretical expression for the ratio $R(\theta)/R_F(\theta)$ in terms of the average electron density gradient along the surface normal is given by

$$\frac{R(\theta)}{R_F(\theta)} = \left| \frac{1}{<\rho_e>} \int_{-\infty}^{\infty} \left\langle \frac{\partial \rho_e}{\partial z} \right\rangle e^{iQ_z z}\, dz \right|^2 \tag{7}$$

in the Born approximation limit, i.e. $\theta >> \theta_c$. This expression has been used extensively to model the reflectivity of liquid crystal/air interfaces where the density is modulated by the "smectic layers" induced by the surface. This same expression has been used to describe the interface of rough surfaces. The derivative of the density with respect to z depends on the length scale over which the roughness is integrated over. This length scale depends on the resolution of the measuring instrument and can vary between several hundred Angstroms to length scales approaching a micron.

Several simple forms for $\rho_e(z)$ and the resulting reflectivities, $R(\theta)/R_F(\theta)$, given by Eq. 7 will be considered.

(i) If ρ_e is a step function, then the derivative is a delta function. Taking the fourier transform of a delta function gives unity and we are left with the desired result that $R(\theta)=R_F(\theta)$.

(ii) If ρ_e is an error function, then the derivative is a Gaussian. In addition, the reflectivity for such an interface deviates from the Fresnel law as a Gaussian, i.e. $R(\theta)/R_F(\theta)=\exp(-\sigma^2 Q_z^2)$.

For many systems a single Gaussian may not be adequate to describe the derivative of the density profile. In such cases the system can be modeled by a density derivative which is the sum of several Gaussians which may be centered at different positions. As we shall see, for simple liquids, the expected reflectivity deviates from the Fresnel form very much like a Gaussian.

Up to now we have considered diffuse interfaces in which there is no in-plane structure. However, this is usually not the case since real systems are

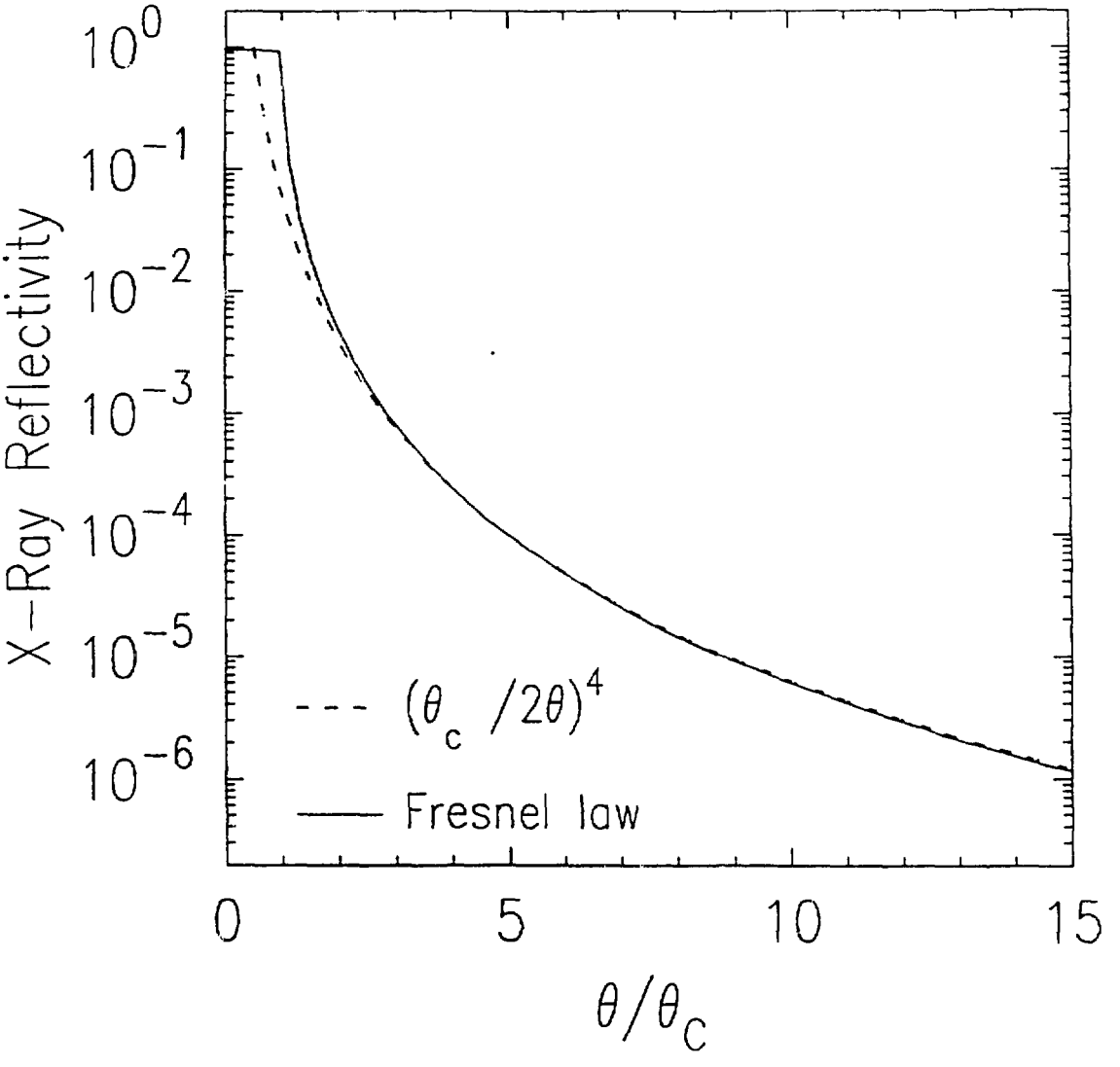

Figure 1. The solid line is the Fresnel law of classical optics and the dashed line is the approximation for $\theta >> \theta_c$: $R_F(\theta) \approx (\theta_c/2\theta)^4$.

"rough". By rough we mean that the height-height correlation is non-zero. In defining the height-height correlation function, the length scale over which we are considering defines the limits of integration. For most systems, the roughness increases as the area of the sampling is increased, hence a "universal" measure of the roughness is inappropriate.

For simple liquids, the height-height correlation function results from thermally excited capillary waves. The two-dimensional energy density for surface waves is made up of a surface tension term, $(\gamma/2)[\nabla_{xy} h(\mathbf{r}_{xy})]^2$, and a gravitational term (important only at long wavelengths),

$$U = \frac{\gamma}{2}\int d^2\mathbf{r}_{xy} \, |\nabla_{xy} h(\mathbf{r}_{xy})|^2 + \frac{\rho g}{2}\int d^2\mathbf{r}_{xy} \, h(\mathbf{r}_{xy})^2 \tag{8}$$

Taking into account the density of states and applying the equipartition theorem one obtains the following expression for the root-mean-squared(r.m.s.) roughness of the free surface due to capillary waves,

$$<h(0)^2> = \frac{k_B T}{4\pi^2\gamma}\int d^2\mathbf{Q}_{xy} \frac{1}{|\mathbf{Q}_{xy}|^2 + k_g^2} \tag{9}$$

where $k_g^2 \equiv \rho g/\gamma$. The upper limit of this integral, $k_{\max}$, is on the order of π/r_M, where r_M is the molecular radius. Without the gravity term, $\rho g/\gamma$, the integral would have an infrared divergence $\mathbf{Q}_{xy} \rightarrow 0$. Using these limits, integration of Eq. 9 results in the following equation for the intrinsic roughness of a liquid surface,

$$<h(0)^2> = \frac{k_B T}{4\pi\gamma} \log\left(\frac{k_{\max}^2 + k_g^2}{k_g^2}\right). \tag{10}$$

For water $<h(0)^2>^{1/2} \approx 3.98$ Å at room temperature[24]. The gravitational length scale, $1/k_g$, is inaccessible with realistic resolution volumes, and the measured, or effective, roughness is larger than the intrinsic roughness.

In this approximation, the reflectivity $R(\theta)$, is given by

$$R(Q_z) = e^{-\sigma_T^2(Q_z)Q_z^2} \tag{11}$$

where $\sigma_T^2 = \sigma_C^2 + \sigma_P^2$. The first term is from thermal capillary waves and the second term is from the finite size of the liquid molecules. Braslau et. al[10] have shown that the capillary term is given by

$$\sigma_C^2(Q_z)Q_z^2 = \frac{k_B T}{2\pi\gamma} Q_z^2 \log\left(\frac{2\pi}{Q_z r_M(\Delta\theta_d)}\right) \tag{12}$$

where r_M is the molecular radius and $\Delta\theta_d = h_d/L$ is the full width of the

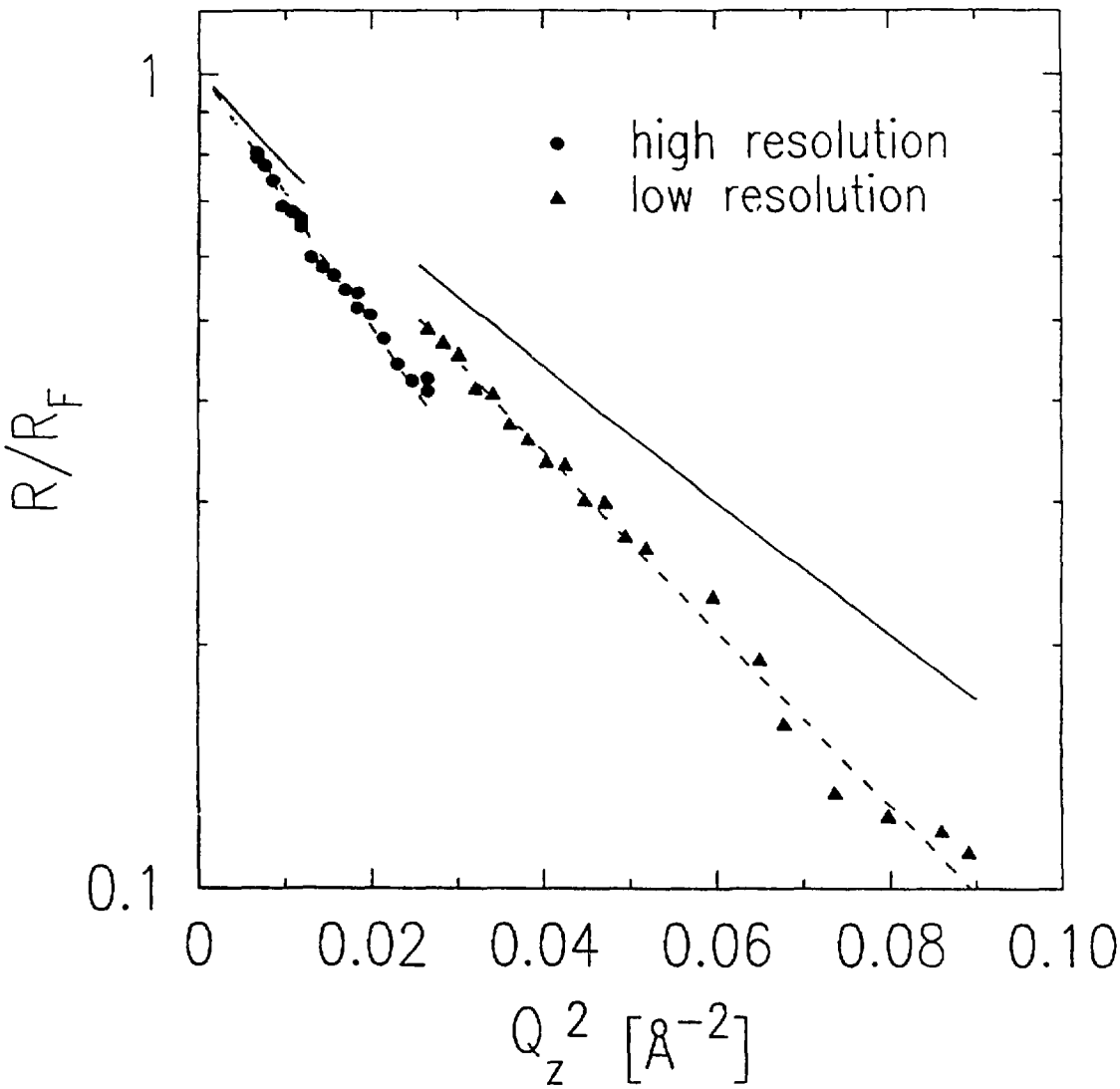

Figure 2. The measured reflectivity of carbon tetrachloride normalized to the Fresnel reflectivity is shown. The solid lines are the predictions of the capillary-wave model for the two resolutions. The dashed lines are the best fit to a surface profile width which is added in quadrature to the capillary roughness.

angular resolution in the plane of incidence.

X-ray Reflectivity studies have been carried out on the free surface of water, carbon tetrachloride, and methanol[10]. As predicted by the capillary wave model the roughness of the interface is higher for the liquids with the smaller surface tensions, i.e. it is easier to excite thermal roughness on surfaces with a smaller stiffness. All of these liquids are in reasonable agreement with the predictions of Eq. 10 and Eq. 11. The data has been fit to a single parameter, σ_P, whereas σ_C has been calculated exactly.

For carbon tetrachloride the reflectivity normalized to R_F is shown in Figure 2. The filled square data is taken with higher resolution then the filled triangle data, therefore, the effective σ_C from Eq 10. is larger and the reflectivity is smaller. The results of the capillary model with σ_P=0 is shown as the solid lines. In order to fit the data, σ_P has been adjusted. For the higher resolution data σ_P=2.5 Å and for the lower resolution data σ_P=3.3 Å. The model with these parameters is shown as dashed curves in figure 2. The data has also been equally fit to a simple Gaussian form

$$R(Q_z) = e^{-\sigma_M^2 Q_z^2} \tag{13}$$

This fit gives a value σ_M=5.13 Å for the higher resolution data and σ_M=5.93 Å for the lower resolution data.

3. DISCRETE MODELS (Au(100) Surface)

We will now turn to the subject of specular reflectivity from crystalline surfaces, and in particular from the (100) surface of gold. In this example, we will consider the "Fresnel" reflectivity which arises from the termination of the crystal as well as the nature of the "Bragg" reflectivity which results from the periodicity of the atomic arrangement. As we shall see, these effects are essentially the same and can not be easily separated from each other.

The Au(100) is believed to exhibit a buckled, slightly rotated triangular structure, incommensurate (in-plane) with the underlying square substrate. This picture has emerged from a variety of experiments and calculations. Initial LEED observations concluded that the overlayer reconstructs with a "(5X1)"[25, 26] Shortly thereafter, Fedak and Gjostein resolved a splitting in the LEED pattern and proposed a "(20X5)" structure with a a hexagonal overlayer on a square substrate. This model corresponds to a ~20% contraction along the direction corresponding to the "(5X1)" reconstruction and a ~5% contraction along the orthogonal surface direction. More recent LEED measurements[27] have resolved additional spots. This same data has been reinterpreted by rotated domains which are nearly 14X5 which is more precisely described by a large unit cell given by c(26X68) reconstruction[28]. Unfortunately, multiple scattering effects have made a definitive determination of the structure impossible so far. The additional ~25% mass required by such an triangular overlayer has been detected by ion scattering[27].

In the kinematical approximation, the scattering can be calculated by summing the cross-section for electrons over the resolution volume. In the

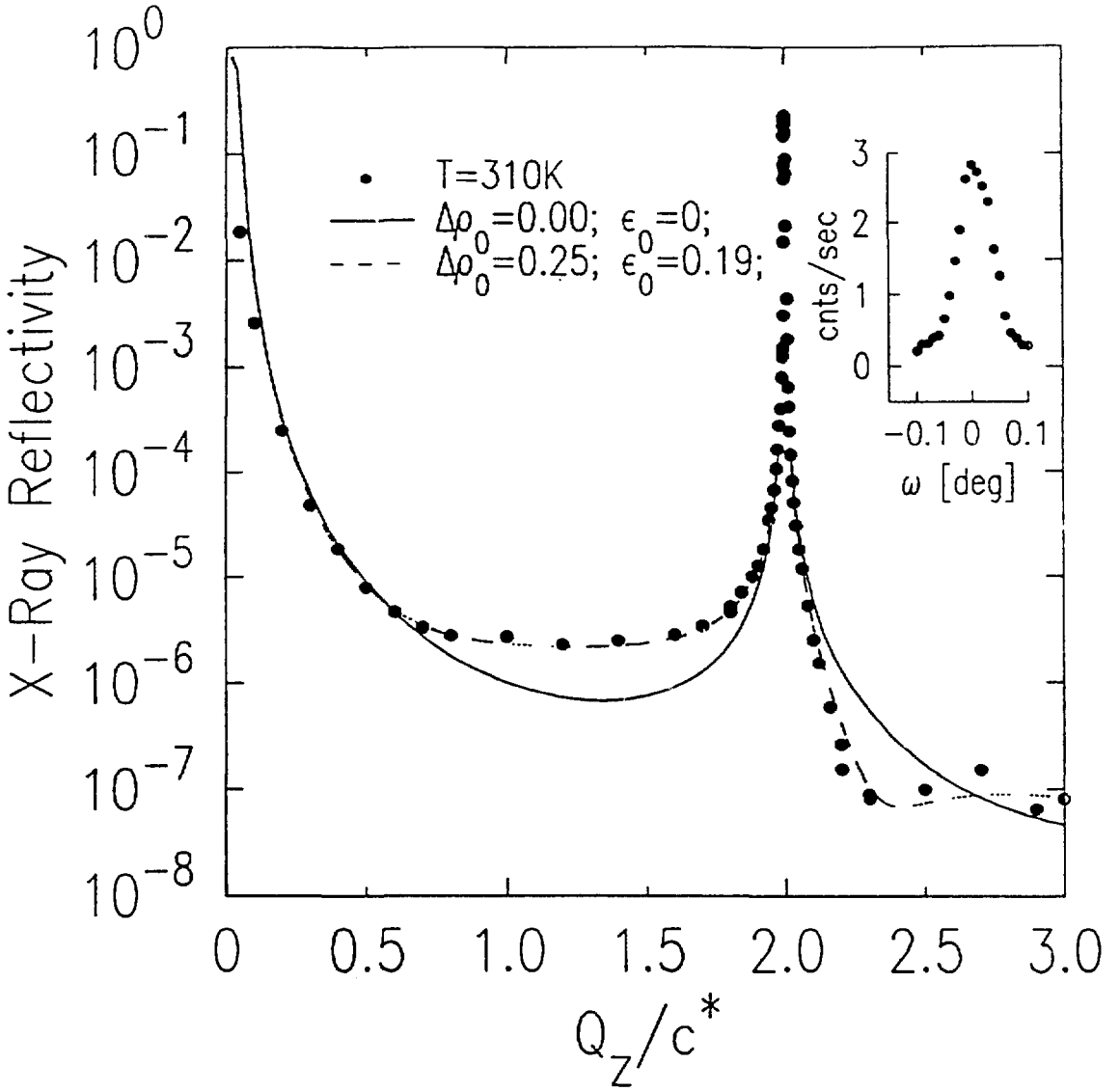

Figure. 3. Specular reflectivity of the clean Au(100) surface normalized to the incident flux at T=310K. The solid line corresponds to a real space model with an ideally terminated bulk as given by Eq. 14. The dashed line correspond to ϵ_0=19%, an increased mass of $\Delta\rho_0$=25%, and a buckling amplitude of ς_0=20% as described by Eqn(16). The inset corresponds to the rocking curve at Q_z/c^*=1.0

case of a perfectly terminated crystalline material, $R(Q_z)$ can be expressed as either a sum over the positions of each atomic layer

$$R=\frac{16\pi^2 r_0^2 T^4(\theta)\,|F(Q_z)|^2 e^{-2W(Q_z)}}{a^4 Q_z^2}\,\Big|\sum_{n=0}^{\infty} e^{iQ_z dn}\Big|^2 \qquad (14)$$

or equivalently as a sum over Bragg peaks[29, 5, 31, 32]

$$R=\frac{64\pi^2 r_0^2 T^4(\theta)\,|F(Q_z)|^2 e^{-2W(Q_z)}}{a^6 Q_z^2}\,\Big|\sum_{(L\ even)} \frac{(-1)^{L/2}}{Q_z - Lc^*}\Big|^2. \qquad (15)$$

In these expressions $d=a/2$ is the layer spacing, The Debye-Waller factor is given by $W(Q_z)$ and the form factor is given by $F(Q_z)$. The $(Q_z-Lc^*)^{-2}$ tails evident in Eq. (15) are familiar in the context of Darwin theory of Bragg reflectivity. Because of the factor $(-1)^{L/2}$, the amplitudes of neighboring peaks add constructively.

Figure 3 displays the specular reflectivity of Au(100) from $Q_z/c^*=0.15$ to $Q_z/c^*=3.5$ at T=310K. The inset shows a typical rocking curve obtained at the anti-Bragg position ($Q_z/c^*=1.0$) at this temperature. Before turning to a more detailed analysis, it is worth noting that the measured reflectivity in Figure 3 extends over a range of nearly seven decades and over scattering angles from $2\theta = 1^\circ$ to 75°, smoothly joining the (002) reflection to the origin. This is all the more impressive in view of the finite reflectivity obtained at the "forbidden" (001) reflection, where successive planes scatter exactly out of phase. Together with the absence of any measurable diffuse scattering in the transverse direction this suggests that on the length scales sampled by the resolution volume, the surface may be both atomically flat and perfectly aligned with the crystallographic planes. To estimate the in-plane coherence area we note that the width of the θ-scan(inset to Figure 3) is only 0.07° FWHM. This corresponds to the 2θ resolution and gives a width in reciprocal space of $\Delta Q_x = Q_z \Delta\omega = 0.001$ Å^{-1}. Because it is very unlikely that a Au surface can be cut to these specifications, we conclude that upon annealing it must rearrange itself to expose smooth (100) facets several thousand Angstrom across. It seems certain that the several thousand Angstrom correlation length is a lower limit because of the contributions to $\Delta\omega$ of "extrinsic" factors, such as the macroscopic sample mosaic (0.02°) and the finite 2θ-resolution.

The most striking feature of the data in Figure 3 is the pronounced asymmetry evident in the reflectivity about the (002) reflection. The solid line in Figure 3 was obtained from Eq. 14 using the known atomic and crystal structure of bulk Au. It is clear that the model's prediction is substantially too low for $Q_z/c^*<2$ and too high for $Q_z/c^*>2$. Nor can the asymmetry be qualitatively understood as resulting from surface damage or contamination. The reflectivity at the anti-Bragg position from a rough surface is generally reduced from that of a smooth surface[29, 30, 31], which is clearly not

supported by the data.

The room temperature data can be described with simple real space models of the surface reconstruction where only the top layer has been modified. In the following we consider three different parameters:

- ϵ_0 - spacing between the top and next layers
- $\Delta\rho_0$ - top layer excess mass density
- $F_0(Q_z)$ - Buckling induced roughness

We modify Eqn. (14) by rewriting the sum as

$$\left| f_0(Q_z)(1+\Delta\rho_0)e^{iQ_z d\epsilon_0} + \sum_{n=1}^{\infty} e^{iQ_z dn} \right|^2 \tag{16}$$

Here $f_0(Q_z)$ represent the Fourier transform of the charge distribution for the top layer. For a buckled top layer in the specular geometry

$$f_n(Q_z) = J_0(Q_z\zeta_n), \tag{17}$$

where J_0 is the zeroth order Bessel function and ζ_n is the buckling amplitude[33, 34]. This form distributes the charge along the surface normal direction by introducing a sinusoidal mass distribution in z into the nth layer, while preserving the center of mass of the layer. For small ζ_n, ie. $Q_z << \zeta_n^{-1}$, the Bessel function and a Gaussian ($f_n(Q_z)=e^{-Q_z^2\zeta_n^2/2}$) are both quadratic and differ only by a scale factor. Best fits to both forms are indistinguishable over the Q_z-range of the existing data. Since the Bessel function form is motivated by a simple real space model, we have chosen to use this form in the analysis. From the present data it is not possible to determine the sine wave period. We have also included a bulk Debye-Waller factor $W(Q_z) = -Q_z{}^2<u^2>/2$ with $\sqrt{<u^2>}$ varying between 0.1 Å and 0.2 Å. Such values are appropriate for bulk Au in the temperature range studied.

The most important result from the least squares fitting is that of the three parameters (ϵ_0, $\Delta\rho_0$, and ζ_0) only the variation of ϵ_0 can produce the observed asymmetry. The dashed line in Figure 3 shows the best fit obtained by varying $\Delta\rho_0$, ϵ_0, and ζ_0 (and including all the data). This model, which gives an excellent fit, has an expansion of ϵ_0=19%, an increased mass of $\Delta\rho_0$=25%, and a buckling amplitude of ζ_0=20%. It is noteworthy that the increased mass is consistent with the 5×20 model of Zehner[27]. The measured expansion, combined with the increased mass of the top layer, gives a mass density which is close to the bulk value.

It is interesting that no surface roughness has been required to fit the data, supporting the suggestion that the clean, annealed surface is atomically smooth over regions of at least several thousands of Angstroms in extent. In contrast, one would expect roughness to be important in a description of damaged or contaminated surfaces. Examples of these are shown in Figure 4. The reflectivity is very much lower near the anti-phase position than for the clean room temperature data. Near the Bragg peak the three data sets agree more

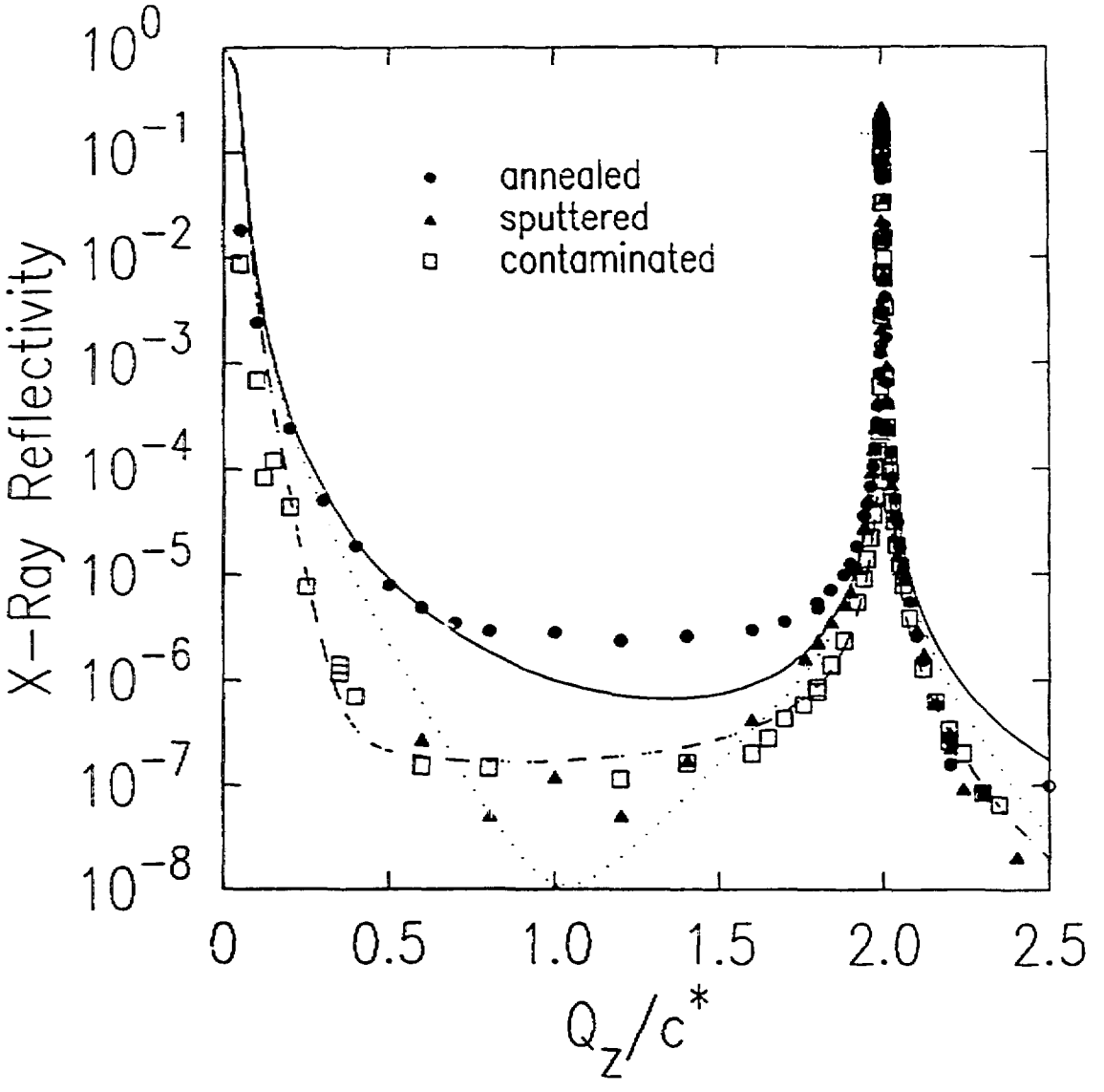

Figure 4. Specular reflectivity of the clean Au(100) surface at room temperature (filled circles), of a surface exposed to atmosphere for > 24 hours and then heated to 690K (open squares), and of a clean surface sputtered for 50 minutes at T=300K (filled triangles). The solid line corresponds to the ideally terminated bulk. The dotted line is the result of a roughness model given by Eq. 18 as described in the text. The dashed line is the result of a fit to Eq. 19.

closely, although not perfectly.

Several models have been considered to fit the annealed and sputtered data shown in Figure 4. In the first model, we have allowed for a variable occupation in the density of successive layers according to an error-function distribution. This is the discrete equivalent to the Gaussian model discussed in the previous section. To accomplish this, the sum in Eq. 14 is replaced by

$$\frac{1}{2}\left|\sum_{n=-\infty}^{\infty} 1 - erf\left(\sigma(dn - z_0)\right)e^{iQ_z dn}\right|^2 \tag{18}$$

where σ is the width of the distribution and z_0 is the position. For this model it is assumed that all of the atomic layers are uniformly spaced. The results of this model with σ=3 Å and z_0=1.5 Å is shown as the dotted curve in Figure 4. This model does not adequately describe the contaminated or sputtered data.

Rather than construct an elaborate real space model, we have chosen to modify the sum of Eq. 15 to include two charge-density waves.

$$\left|\frac{e^{-\sigma_0^2 Q_z^2/2}}{Q_z} - \frac{e^{2\pi i\phi}e^{-\sigma_2^2(Q_z - 2c^*)^2/2}}{Q_z - 2c^*}\right|. \tag{19}$$

One density wave corresponds to Q_z=0 and the other corresponds to $Q_z = 2c^*$ which should be sufficient in the region relevant to our experiments. Each, however, is modified by its own Gaussian of widths, σ_0 and σ_2, respectively. In simple models[10], σ_0 can be identified with the r.m.s. roughness of the interface between the metal and the vacuum, while σ_2 is the r.m.s. roughness of the interface between the ideally terminated crystal and the overlayer above it. We allow for a variable phase, ϕ which for perfect termination is zero (Eq. (18)). The fit of the reflectivity data from a surface exposed to air for > 24 hours (open squares) to this form (dashed line) is shown in Figure 4. The best fit parameters are ϕ=0, σ_0=4.5 Å, σ_2=0.5 Å, and $\langle u^2\rangle^{1/2}$=0.25 Å. Thus, we arrive at the physically appealing picture of a damaged, rough surface layer (r.m.s. roughness 4.5 Å), in which Au atoms are not positioned in lattice planes and are separated from the undamaged bulk by a relatively smooth interface (0.5 Å r.m.s. roughness).

In summary, by the use of absolute reflectivity techniques we have shown that atomically smooth Au(100) facets may be prepared over length scales of several thousand Angstroms. The asymmetric angular dependence of clean annealed surfaces is consistent with an expanded, possibly buckled, hexagonal surface structure. A more sophisticated analysis of the out-of-plane structure will accompany future in-plane studies.

4. LIQUID/SOLID INTERFACES (8OCB)

Due to the penetrating nature of x-rays, the characteristics of a liquid/solid interfaces can also be investigated using x-ray reflectivity

techniques. In this case, the scattering/reflectivity must be considered upon entering the fluid layer and upon impinging on the liquid/solid interface. In order to account for absorption losses in the liquid layer, it is important to utilize a geometry where these effects can be understood simply. Therefore, we have chosen a cylindrical "transmission" geometry for these reflectivity measurements. In this geometry, the liquid is placed in a cylinder which is of the order of the x-ray absorption length. For molybdenum radiation(λ=0.71 Å) and for hydrocarbons the absorption length is ~1 cm. Within the liquid immersed cylindrical sample cell there is a concentric silicon disk. The x-rays enter the liquid and are then reflected from the liquid/silicon interface because of the change in the index of refraction in going across the interface.

Since the sample is rather small by reflectivity standards, we were not able to limit the incident beam size to avoid the extremes of the x-ray beam from spilling over the sample. Instead, it was assumed that the incident flux scaled as the incident angle and the reflectivity was appropriately scaled. The intensity scale factor was obtained by least-squares analysis.

In figure 5(circles), the measured reflectivity is shown for the liquid crystal material 4-cyano-4'octyloxybiphenol(8OCB) at the interface of an alkylsiloxane monolayer on a silicon substrate at T= 66.6 ° C. We have chosen to study 8OCB since surface effects have been very well characterized at the air/liquid interface by Pershan and coworkers[11]. At this temperature, 0.3 ° C above the bulk smectic phase, there is smectic layering induced by the interactions with the alkylsiloxane surface. The dashed line in figure 5 is the expected reflectivity from Eq. 4 using the critical angle for the silicon substrate($q=4\pi/\lambda\sin[\theta]$). This is what would be expected at small q-vectors from the air/silicon interface. This model does not agree with the data since the dielectric constant of the liquid is not unity.

The actual change in the dielectric constant(free electron density) at the liquid crystal/silicon interface is considerably smaller then for the air/silicon interface. Since the critical angle scales as the square root of the density change, it can be shown that the critical angle at the liquid/solid interface is given by

$$q_c^2[l/s]=q_c^2[s]-q_c^2[l] \tag{20}$$

where $q_c[l/s]$ is the critical wavevector of the liquid/solid interface, $q_c[s]$ is the critical wavevector of the solid, and $q_c[l]$ is the critical wavevector of the liquid. For the silicon/8OCB interface, q_c[silicon]=0.0316 Å^{-1} q_c[8OCB]=0.0217 Å^{-1} and q_c[8OCB/silicon]=0.0230 Å^{-1}. The Fresnel law, given by Eq. 4 with $\theta_c=q_c$[8OCB/silicon]($\lambda/4\pi$) is shown as the dotted line in figure 5. At small q-vectors the data agrees very well with the predictions of the model. At q-vectors of order 0.2 Å^{-1} there are deviations between the Fresnel law and the data. This can be understood in terms of the smectic layering induced by the broken symmetry at the interface. As the nematic to smectic A transition temperature is approached this peak increases in intensity and narrows corresponding to an increasing number of surface smectic layers. This result clearly demonstrates that the x-ray reflectivity technique is applicable at a liquid/solid interface.

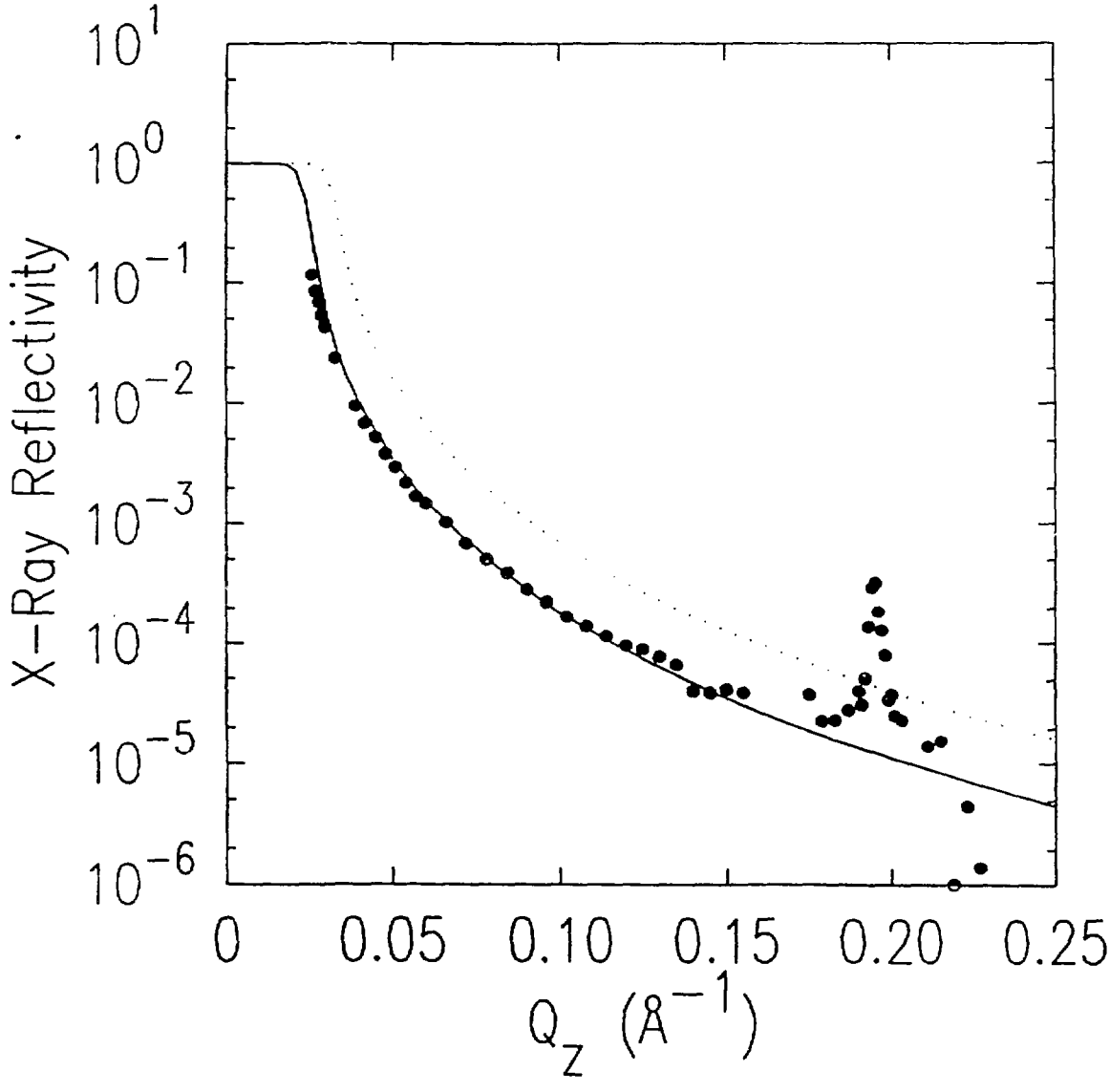

Figure 5. Specular reflectivity of the interface between the liquid crystal 8OCB and an alkylsiloxane coated silicon surface(circles). The dashed line is the Fresnel law with the critical angle of silicon(q_c=0.317 $Å^{-1}$). The solid line is the Fresnel law with the critical angle for the 8OCB/silicon interface(q_c=0.230 $Å^{-1}$). The deviation between the solid line and the data at ~0.2 $Å^{-1}$ is a consequence of smectic layering at the interface.

5. SUMMARY

The technique of X-ray reflectivity provides detailed information about the structure along the surface normal direction. In this paper we have considered air/liquid, vacuum/solid, and liquid/solid interfaces. The ability to probe liquid/solid interfaces should be particularly valuable in understanding the electrode/electrolyte interface in the future.

The measurements on CCl_4 were done in collaboration with A. Braslau, P.S. Pershan, G. Swislow, and Jens Als-Nielsen. These measurements were in part supported by grants from the U.S. National Science Foundation through grants DMR-85-13523 and DMR-86-14003, from the Joint Services Electronics Program through grant N00014-75-C-0648, the Danish National Science Foundation, and the RIS National Laboratory. The measurements on Gold were done in collaboration with Doon Gibbs, S.G.J. Mochrie, and D.M. Zehner. The experiments on the liquid crystal/solid interfaces were done in collaboration with Larry Sorensen. Work performed at Brookhaven National Laboratory is supported by the Division of Materials Research, U.S. Department of Energy, under Contract No. DE-AC02-76CH00016.

References

1. Richard Hoffman, NATO Advanced Study Institute on Spectroscopic and Diffraction Techniques in Interfacial Electrochemistry.
2. L. Blum, H.D. Abruna, J. White, J.G. Gordon, G.L. Borges, M.G. Samant, and O.R. Melroy, *J. Chem. Phys.*, vol. 85, p. 6732, 1986.
3. G. Materlik, J. Zagenhagen, and W. Uelhogg, *Phys. Rev. B*, vol. 32, p. 5502, 1985.
4. Mahesh G. Samant, Michael F. Toney, Gary L. Borges, Lesser Blum, and Owen Melroy, *J. Phys. Chem*, vol. 92, p. 220, 1988.
5. I. K. Robinson, *Phys. Rev. B*, vol. 33, p. 3830, 1986.
6. L. Bosio and M. Oumezine, *J. Chem. Phys.*, vol. 80, p. 959, 1984.
7. B.C. Lu and S.A Rice, *J. Chem. Phys.* , vol. 68, p. 5558, 1978.
8. D. Sluis and S.A. Rice, *J. Chem. Phys.* , vol. 79, p. 5658, 1983.
9. A. Braslau, M. Deutsch, P.S. Pershan, A.H. Weiss, J. Als-Nielsen , and J. Bohr, *Phys. Rev. Lett.*, vol. 54 , p. 114 , 1985.
10. A. Braslau, P.S. Pershan , G. Swislow, B.M. Ocko, and J. Als-Nielsen , *Phys. Rev. A*, vol. 38, p. 2457, 1988.
11. P.S. Pershan, A. Braslau, A.H. Weiss, and J. Als-Nielsen , *Phys. Rev. A.*, vol. 35, p. 4800, 1987.
12. B.M. Ocko, A. Braslau, P.S. Pershan , J. Als-Nielsen , and M. Deutsch, *Phys. Rev. Lett.* , vol. 57, p. 94, 1986.
13. E.F. Gramsbergen, W.H. de Jeu, and J. Als-Nielsen, *J. Phys.(paris)*, vol. 47, p. 711, 1986.

14. D.K. Schwartz, A. Braslau, B.M. Ocko, P.S. Perhsan, J. Als-Nielsen, and J.S. Huang, *Phys. Rev. A*, 1988. accepted for publication
15. C.A. Helm, H. Mohwald, K. Kjaer, and J. ALs-Nielsen, *Europhys. Lett.*, vol. 4, p. 697, 1987.
16. S.G. Wolf, L. Leiserowitz, M. Lahev, M. Deutsch, K. Kjaer, and J. Als-Nielsen, *Nature*, vol. 328, p. 63, 1987.
17. R.M. Richardson and S.J. Roser, *Liquid Crystals*, vol. 2, p. 797, 1987.
18. Doon Gibbs, B. M. Ocko, D. M. Zehner, and S. G. J. Mochrie, *Phys. Rev. B*, vol. 38, p. 7303, 1988.
19. B. M. Ocko and S. G. J. Mochrie, *Phys. Rev. B*, vol. 38, p. 7378, 1988.
20. R.A. Cowley and T.W. Ryan, *J. Phys. D; Appl. Phys.* vol. 20, p. 61, 1987.
21. M. Pomerantz, A. Segmuller, L. Netzer, and J. Sagiv, *Thin Solid Films*, vol. 32, p. 153, 1985.
22. I.M. Tidswell, B.M. Ocko, P.S. Pershan, S.R. Wasserman, G.W. Whitesides, and J.D. Axe. submitted to Phys. Rev. B
23. J.D. Jackson, in *Classical Electrodynamics*, p. 281, John Wiley & Sons(New York), 1975.
24. R. Loudon, "Riples on Liquids Interface," in *Surface Excitations*, ed. V.M. Agranovich and R. Louden, p. 589, Elsevier Science Publishers B.V., 1984.
25. D.G. Fedak and N.A. Gjostein, *Phys. Rev. Lett.*, vol. 16, p. 171, 1966.
26. A.M. Mattera, R.M. Goodman, and G.A. Somorjai, *Surf. Sci.*, vol. 7, p. 26, 1967.
27. D. M. Zehner, B. R. Appleton, T. S. Noggle, J. W. Miller, J. H. Barret, L. H. Jenkins, and O. E. Schow III, *J. Vac. Sci. Technol.*, vol. 12, p. 454, 1975.
28. M.A Van Hove, R.J. Koestner, P.C. Stair, J.B. Biberian, L.L. Kesmodel, I. Bartos, and G.A. Somorjai, *Surf. Sci.*, vol. 103, p. 189, 1981.
29. S.R. Andrews and R.A. Cowley, *J. Phys C*, vol. 18, p. 6427, 1985.
30. D.A. Bruce, *J. Phys. Chem C*, vol. 14, p. 5195, 1981.
31. A.M. Afanas'ev, P.A. Aleksandrov, S.S. Fanchenko, V.A. Chaplanov, and S.S. Yakimov, *Acta. Cryst. A*, vol. 42, p. 116, 1986.
32. I. S. Gradshteyn and I. M. Ryzhik, *Table of Integrals, Series, and Products*, p. 36, Academic Press, New York, 1965. By including an infinitesimal imaginary component to Q_z this sum can be performed exactly: $\left|\sum_{n=0}^{n=\infty} e^{iQ_z dn}\right|^2 = |1/\sin(Q_z d/2)|^2$. Then using Eqn. (1.422.3) of this reference i.e. $1/\sin\pi z = \frac{1}{\pi}\sum_{n=-\infty}^{n=\infty}(-1)^n/(z-n)$, we obtain our Eq. (15).
33. J.D. Axe, *Phys. Rev. B*, vol. 21, p. 4181, 1980.
34. One obtains a zeroth order Bessel function if $Q_x = Q_y = 0$.